



Anisotropic Molecular Hopping at the Solid-Nematic Interface

Journal:	<i>Soft Matter</i>
Manuscript ID:	SM-COM-05-2015-001251.R1
Article Type:	Communication
Date Submitted by the Author:	04-Aug-2015
Complete List of Authors:	Chakraborty, Saonti; University of Colorado, Boulder, Chemical and Biological Engineering Nelson, Nathaniel; University of Colorado, Boulder, Chemical and Biological Engineering Schwartz, Daniel; University of Colorado, Boulder, Chemical and Biological Engineering

Anisotropic Molecular Hopping at the Solid-Nematic Interface

Saonti Chakraborty, Nathaniel Nelson, and Daniel K. Schwartz^{*}

Department of Chemical and Biological Engineering
University of Colorado Boulder, Boulder, CO 80309

^{*}To whom correspondence should be addressed: daniel.schwartz@colorado.edu

Abstract

Single molecule tracking was used to observe intermittent and anisotropic molecular motion at the solid–nematic interface. Although the interfacial diffusion was dramatically slower than self-diffusion in the nematic, the diffusion anisotropy was the same at the interface and in bulk, supporting the desorption-mediated mechanism of interfacial diffusion, where molecules sample the physical properties of the vicinal fluid phase during flights, and the magnitude of the interfacial diffusion coefficient is primarily determined by the distribution of waiting times between flights.

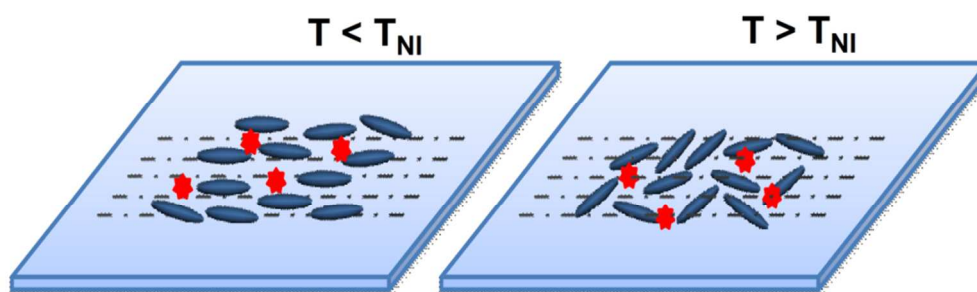


Table of Contents Figure

Liquid–solid interfaces are ubiquitous in many physical, chemical, and biological systems, and play crucial roles in a variety of applications¹ including self-assembly, catalysis, tribology, membrane biophysics, crystal growth, and biosensing to name a few. Liquid–solid interfaces are also of fundamental interest, since molecular-level interactions with the solid surface result in unique dynamics that may be dominated by either of the bulk phases or may substantially deviate from both. Recent single-molecule tracking experiments have demonstrated that molecules at interfaces exhibit intermittent motion^{2, 3}, where they undergo sequences of confined surface diffusion (“waiting” periods) alternating with “flights”, which can be large. It has been hypothesized that these flights comprise desorption from the surface followed by three dimensional diffusion through the bulk liquid, and reattachment at a new location on the surface, and a number of observations have indirectly supported this mechanism^{4, 5}. Mathematically, this motion can be represented using a model known as a continuous-time random walk (CTRW)⁶ which is a generalized version of random walk behavior where the metronomic motion of the random walk is replaced by a distribution of waiting times, and the constant step size of the random walk is replaced by a “flight length” distribution, which is generally heavy-tailed and includes the possibility of long Lévy flights.

Here, we test the desorption-mediated interfacial diffusion hypothesis directly, by comparing the motion of molecules under conditions where the solid surface remains exactly the same, and the adjacent fluid phase is either isotropic or anisotropic. This is accomplished by using a liquid crystal material (LCs) as the fluid. LCs are a unique class of soft materials with structural and dynamic properties that combine the “fluidity” of liquids and the “anisotropy” of crystalline solids. These properties, combined with the fact that LC orientation can be controlled using

external fields or interfacial properties makes them uniquely useful for many applications ⁷ such as displays (LCDs), sensors, and electro optical and biomedical devices. More generally, the orientational and spatial ordering of LC materials on surfaces gives rise to a variety of physical behavior ⁸, and is also relevant to many biomolecular processes ⁹.

We have used high-throughput single-molecule total internal reflection fluorescence (TIRF) microscopy to study of the diffusion of individual molecules at the interface between a modified sapphire surface and the uniaxial nematic mesogen, 4-Cyano-4'-pentylbiphenyl (abbreviated as 5CB). The solid surface was carefully treated, as described below, to align the nematic phase uniformly in a specific direction relative to the laboratory coordinates. The uniaxial nematic phase is the simplest liquid crystalline phase, exhibiting macroscopic orientational order that is described by the nematic director \vec{n} . Diffusion in a bulk nematic phase is described by the principal components of the second-rank diffusion tensor (\vec{D}) with D_{\parallel} and D_{\perp} , defined for motion parallel and perpendicular with respect to the director \vec{n} , respectively.

Transport processes in bulk LC phases have been extensively studied for over thirty years. Anisotropic diffusion coefficients, parallel and perpendicular to the director, have been quantitatively measured in thermotropic and lyotropic systems by means of techniques such as forced Rayleigh scattering (FRS) ¹⁰ and nuclear magnetic resonance (NMR) ¹¹. Recently, fluorescence methods have been used to investigate the dynamics of small molecules in bulk LCs ¹². For instance, fluorescence correlation spectroscopy (FCS) ¹³ and fluorescence recovery after photobleaching (FRAP) ¹⁴ have been used to determine apparent mean diffusion coefficients in bulk nematic and free-standing LC films of different thicknesses. Moreover, single molecule

experiments have also been implemented to investigate the structure and dynamics of LCs in restricted geometries and in thin films¹⁵. In contrast to these measurements, TIRF microscopy has the ability to track the motion of large numbers of individual molecules and hence, reveal the detailed mechanisms of interfacial mobility.

5CB (4-Cyano-4'-pentylbiphenyl, Alfa Aesar, USA) was used as a nematogen and AlexaFluor 647 (Life Technologies, USA) as a fluorescent probe molecule. Figures 1a and 1b show the respective chemical structures. The size of the probe molecule is similar to that of the 5CB molecules and, therefore, expected to mimic the motion of the liquid crystals and reflect the self-diffusion of the liquid crystal without distorting the director field¹⁶. The fluorophore was added at a very low concentration ($\sim 10^{-10}$ M) directly to the 5CB melt (at ~ 40 °C) and sandwiched between the two bounding surfaces of our TIRF cell – a 2” diameter sapphire wafer (Precision-Micro Optics, USA) and a 1” diameter fused silica coverslip (Mark Optics, USA). Sapphire was chosen as a substrate because of its high refractive index (~ 1.76 at 640 nm) that provided the appropriate optical conditions for total internal reflection at the interface with 5CB.

Both the sapphire and fused silica surfaces were cleaned and coated with a monolayer of (3-Glycidoxypropyl)methyldiethoxysilane (GPTMS, Sigma Aldrich) to induce planar anchoring, where the nematic director is perpendicular to the surface normal (i.e. the molecules “lie down” on the surface). Both the surfaces were mechanically rubbed using a frosted glass stopper in order to obtain uniform planar alignment of the LC molecules along the direction of rubbing and assembled such that the easy axes of the LC on both surfaces were along the same direction. A detailed discussion of our sample and surface preparation procedures are presented in the

Supplementary Information (ESI) ¹⁷. A cartoon of the modified sapphire surface along with the liquid crystal–probe molecule matrix is shown in Figure 1c.

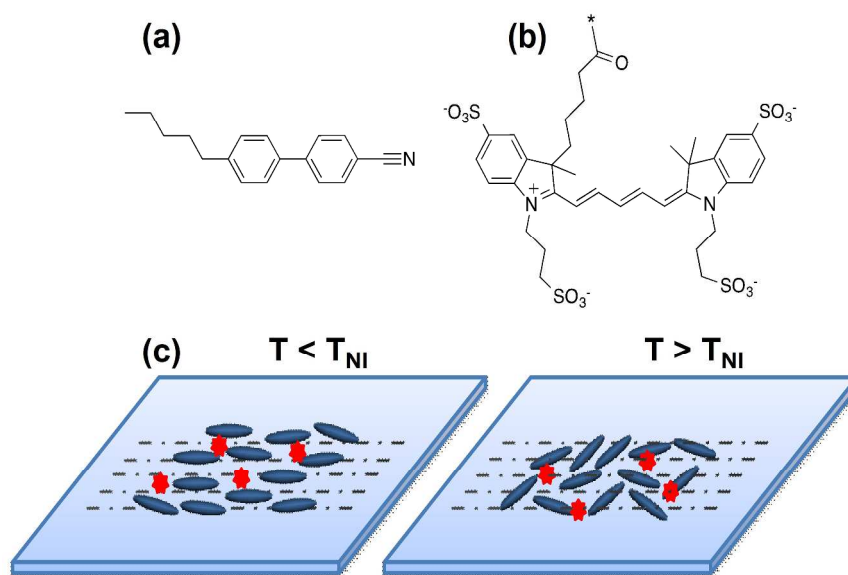


Figure 1. Chemical structures of (a) mesogen 4-Cyano-4'-pentylbiphenyl (5CB) and (b) fluorescent probe AlexaFluor 647. (c) Schematic representation of the 5CB-sapphire interface inside the TIRF cell, shown above and below the nematic-to-isotropic transition in order to indicate the alignment of the 5CB molecules.

The measurements were performed using a custom-built prism-based TIRF microscope (Nikon TE-2000) that was previously described ⁴. The 640nm excitation light was provided by a diode pumped solid state laser (Crystal Laser, model DL-640-100-O). The sample temperature was regulated to within 0.2 °C by an INSTEC STC200 temperature controller. During the experiment, 5CB was aligned by heating the sample directly to the isotropic phase (~40 °C) and cooling slowly to the desired nematic temperature. During the cooling cycle, time sequences of images were recorded every 1 °C until the sample began to crystallize. At every temperature, image sequences were collected using a cooled EMCCD camera (Andor iXon3) for 4 min with an acquisition time of 200 ms per image. Captured images were processed using Mathematica-

based custom image analysis code⁴. Probe molecules in the bulk 5CB diffused much faster (by 2-3 orders of magnitude) compared to those at the liquid-solid interface, so molecules could be resolved only when they adsorbed to the solid surface where they appeared as diffraction-limited spots. Molecular trajectories were constructed by first identifying the centers of intensity of individual bright spots and linking them together in sequential images. Only trajectories that were longer than 10 steps (e.g. 2 sec) were included in the analysis. Directional diffusion coefficients (D_{\parallel} and D_{\perp}) were determined by extracting the positions of the fluorescent molecules from the recorded time-lapse movie, calculating the displacements from these positions, and projecting the displacements into parallel and perpendicular components with respect to the rubbing direction. Finally, the cumulative square displacements were calculated for each component as previously described⁴. Additional details of the TIRF microscope set-up, sample cell geometry, surface preparation and data analysis specific to our system are given in the ESI¹⁷.

We accumulated 40,000-60,000 molecular trajectories for each temperature point. Figures 2a and 2b show representative sets of the trajectories at two different temperatures, above and below the nematic-to-isotropic transition (T_{NI}). As illustrated in these figures, some of the trajectories appeared completely stationary or confined, while others exhibited intermittent behavior, wherein they alternated between periods of confinement and motion ("hops") from one location on the surface to another. As previously reported¹⁸, the intermittent nature of the trajectories resulted in distinctive "step-size" distributions with a narrow central peak (representative of confinement periods) and broad tails (indicating the long hops), as shown in the ESI (Figure S1). For easy comparison, all trajectories were adjusted so that the direction of the local director in

each case was parallel the x-axis. The trajectories in Figure 2a (associated with the nematic phase) in general, appeared to be stretched along a particular direction. On the other hand, trajectories associated with the isotropic phase exhibited no clear directional bias, as shown in Figure 2b. This was qualitative visual evidence of anisotropic surface diffusion in contact with the nematic phase. Moreover, the absence of anisotropic motion at the interface between the exact same solid surface and the isotropic phase proved that the anisotropic motion at lower temperatures was not a consequence of the subtly anisotropic structure imparted to the surface by the mechanical rubbing required to align the LC material. Combined, these observations strongly suggest that the probe molecules “sample” the structure of the neighboring fluid phase during the course of the interfacial motion.

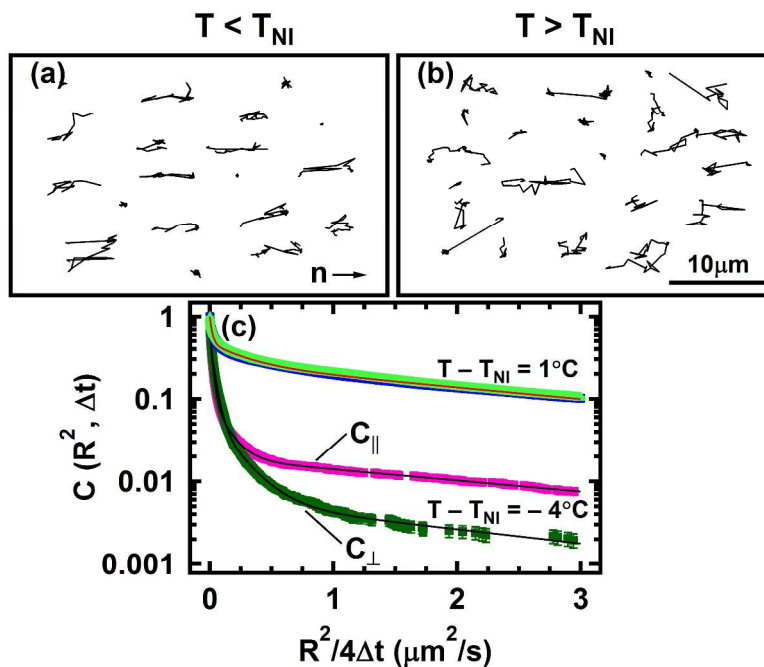


Figure 2. Representative trajectories showing molecular diffusion at the interface between a solid substrate and 5CB illustrating the intermittent nature of the dynamics in the (a) nematic and (b) isotropic phases. (c) Cumulative probability distribution of the squared displacement divided by $4\Delta t$, where $\Delta t = 200$ ms is the lag time between successive image acquisitions. Components $C_{||}$ and C_{\perp} represent the parallel and perpendicular components of the cumulative probability distributions. Black solid lines represent the fits to the data based on equation 1.

Figure 2c shows the cumulative probability distributions of squared displacements⁴ of the probe molecules projected in directions parallel ($C_{||}$) and perpendicular (C_{\perp}) to the rubbing direction, plotted on a logarithmic axis versus $\frac{r^2}{4\Delta t}$. The plots are shown for the isotropic phase ($T - T_{NI} = 1^\circ\text{C}$) and one representative nematic temperature ($T - T_{NI} = -5^\circ\text{C}$). The complete set of all the cumulative square displacement distributions for the rest of the temperature points are shown in Figure S2 of the ESI¹⁷. These data give the probability that the squared displacement of a diffusing molecule will be equal to or larger than $\frac{r^2}{4\Delta t}$ during the time interval $\Delta t = 200$ ms, which is the lag time between successive image acquisitions. In the case of simple Brownian motion,

the cumulative probability distribution of squared displacements would appear as a straight line on this graph, the slope of which would be inversely proportional to the negative inverse of the diffusion coefficient. However, the cumulative probability distribution plots in Figure 2c clearly indicated the presence of multiple diffusive modes for both parallel and perpendicular components. As in previous work, the probability distribution was fitted to a Gaussian mixture model⁴

$$C(r^2, \Delta t) = \sum_i f_i e^{-\frac{r^2}{4D_i\Delta t}}, \quad (1)$$

where, $C(r^2, \Delta t)$ is the cumulative probability of squared displacements, f_i is the fraction of steps associated with mode i and D_i is the characteristic diffusion coefficient corresponding to mode i . The data analyzed here were well-described by a sum of two Gaussians, representing two distinct diffusive modes for interfacial motion. The faster and slower modes corresponded to the “hopping” and “confined” modes, respectively. In the isotropic phase, the fitted diffusion coefficients for the two orthogonal directions coincided quantitatively, exactly as expected for motion at the interface between a solid material and an ordinary liquid. As the system was cooled to $T < T_{NI}$, diffusion became anisotropic with two distinct components, measured for displacements parallel and perpendicular to the rubbing direction. The absolute values of the fitted diffusion coefficients for the slow mode were close to limit of resolution (0.01–0.02 $\mu\text{m}^2/\text{s}$) and were independent of temperature.

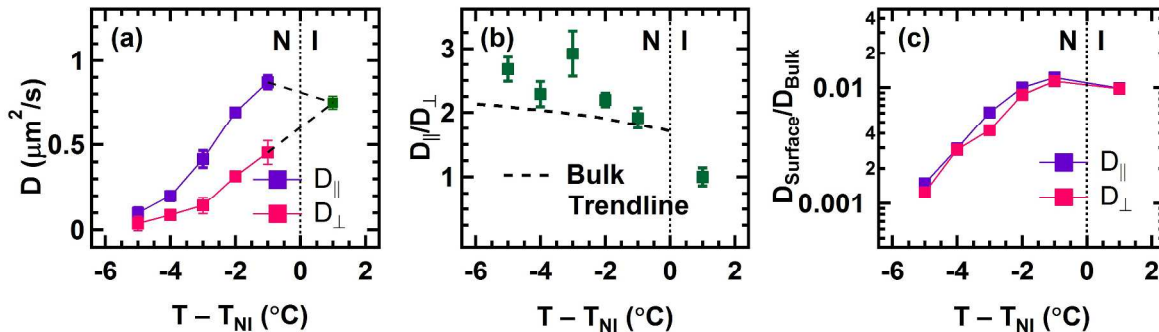


Figure 3. (a) Temperature dependence of the diffusion coefficient in the isotropic phase D_{iso} (green square) and the parallel ($D_{||}$) and perpendicular (D_{\perp}) components (filled symbols) with respect to rubbing direction (which defined the nematic). (b) Temperature dependence of the diffusion anisotropy ($\frac{D_{||}}{D_{\perp}}$). (c) The ratio of the surface to bulk diffusion coefficients as a function of temperature. The bulk diffusion anisotropy profile and self-diffusion coefficients for 5CB were obtained from Ref. ¹¹.

However, the characteristic diffusion coefficients associated with the faster “hopping” mode were distinctly different in the parallel and perpendicular directions and varied with temperature (for $T < T_{NI}$). (Please refer to Tables S1 and S2, and Figure S3 of the ESI ¹⁷ for detailed fit results).

The temperature dependence of the parallel and perpendicular components of “hopping” diffusion coefficients are shown in Figure 3a. In the isotropic phase, where the cumulative distribution plots coincided, diffusion was characterized by a single diffusion coefficient D_{iso} . In the nematic phase, however, two distinct diffusion coefficients, $D_{||}$ and D_{\perp} , were determined. In all cases, $D_{||} > D_{\perp}$, as is the case for diffusion in the bulk nematic phase of 5CB ¹¹. Slightly below T_{NI} , the anisotropic diffusion coefficients bracketed the diffusion coefficient in the

isotropic phase, i.e. $D_{\parallel} > D_{\text{iso}} > D_{\perp}$. However, as temperature was further decreased by ~ 5 °C, D_{\parallel} and D_{\perp} both decreased by nearly an order of magnitude.

To quantify the anisotropy within the nematic phase, we calculated the ratio $\frac{D_{\parallel}}{D_{\perp}}$ (i.e. the “diffusion anisotropy”), as a function of temperature. As shown in Figure 3b, this ratio increased from 1.9 at the highest nematic temperature to 2.7 at the lowest nematic temperature. Interestingly, these values are very similar to the bulk diffusion anisotropy values for nematic 5CB¹¹, which are represented by the dashed line in Figure 3b. (This dashed line indicates a fitted function that was used to represent the measured diffusion anisotropy values in Ref.¹¹). The barely significant discrepancy between the bulk and surface diffusion anisotropies may be due to the dramatic difference in measurement methods (and hence length scales), i.e. NMR vs. molecule tracking, or may be a real physical effect that is a consequence of enhanced nematic order in the interfacial region. Indeed some previous work has suggested that molecular mobility can be anomalous with a few molecular diameters of an interface.¹⁴ However, given the relatively large hops observed (often several hundred nm), it is expected that molecular excursions from the surface generally sample regions of the LC phase that are much farther from the surface, and these extreme near-surface effects would be expected to have only a very small effect.

The absolute values of the interfacial “hopping” diffusion coefficients, however, were nearly two orders of magnitude smaller than the respective values of D_{\parallel} and D_{\perp} for self-diffusion in bulk nematic 5CB¹¹. Moreover, the interfacial diffusion coefficients slowed down much faster than the self-diffusion coefficients with decreasing temperature. Specifically, the ratio of the surface

to bulk diffusion coefficients shown in Figure 3c decreased from $\sim 10^{-2}$ at the highest nematic temperature to 10^{-3} near the crystal transition, implying that the interfacial diffusion coefficients slowed down by almost an order of magnitude relative to the bulk self-diffusion coefficients. A likely explanation for this observation involves an increase in the extent of interaction between the probe molecules and the surface with decreasing temperatures. In the context of the desorption-mediated surface diffusion model, the strength of the molecule-surface interaction (for e.g. van der Waals and dipole-dipole interactions) directly influences the durations of the “waiting times” between successive flights as discussed below in greater detail.

To describe the observations of interfacial diffusion in the context of desorption-mediated interfacial diffusion², we characterized the intermittent behavior of the trajectories by calculating the distribution of waiting times, τ_{des} , between consecutive diffusive steps. The threshold distance of 200 nm described above was used to differentiate between periods of surface displacement and immobilization/confinement. Interestingly, as shown in Figure 4a, these distributions exhibit broader tails at lower temperatures, i.e. long waiting times are more commonly observed at lower temperatures than at higher temperatures.

Theoretically, the distribution of waiting times depends on the underlying cause of immobilization. For example, in the hypothetical case of immobilization due to a single well-defined binding energy, the waiting time distribution $\psi(\tau_{des})$ would be represented by a single decaying exponential function (first order desorption kinetics), whereas, immobilization due to a spectrum of binding energies, $\psi(\tau_{des})$ results in a broad distribution of waiting times that can, in principle, be described by a superposition of decaying exponential processes¹⁸. In fact, we found

that the data could be represented adequately by exponential mixture models employing between three (at the higher temperatures) and five (at the lower temperatures) exponential terms. However, in systems displaying intermittent kinetics (such as, switching between immobility and mobility) over a wide range of timescales, a power law distribution is often used to describe $\psi(\tau_{des})$

$$\psi(\tau_{des}) \sim \tau_{des}^{-(1+\alpha)} \quad (2)$$

This is a special case of the familiar phenomenon of “1/f noise”, which can be due to the superposition of broad distribution of activation energies¹⁹. Equation 2 provided satisfactory fits to the waiting time distributions at all temperatures, as shown in Figure 4a. The fitted value of the only variable parameter, α , decreased systematically with decreasing temperature. The dashed lines in the plot represent power-law fits to the distributions at the highest and lowest temperatures annotated with the fitted values of the exponent. Although the absolute values of the exponents do not have an obvious physical meaning²⁰, the parameters provide a convenient way to quantify the systematic broadening of the experimental waiting-time distribution, and consequently, the longer characteristic waiting times at lower temperatures.

Together, these observations explained the dramatic *absolute* slowing down of the interfacial diffusion coefficients with decreasing temperature, as compared to the bulk diffusion coefficients, despite the fact that the interfacial and bulk diffusion *anisotropy* remained consistent. Specifically, in the context of the desorption-mediated interfacial diffusion model, the *magnitude* of the interfacial diffusion coefficient is primarily determined by the characteristic

waiting times between flights, which are determined by the strength of the molecule-surface interactions. While we are unable to directly observe waiting times shorter than 200 ms in duration (which may, of course, occur during apparent hops), it is likely that the stronger molecule-surface interactions at lower temperatures that are illustrated in Figure 4b, result in longer characteristic “pauses” even at these un-resolved time scales. However, the flights themselves, while virtually instantaneous relative to the time scales of our measurements, sample the properties of the adjacent bulk fluid phase, and in this case are responsible for the anisotropic diffusion, which is virtually the same as in the bulk fluid.

Single-molecule TIRF microscopy was applied to provide direct evidence of anisotropic diffusion at the solid–nematic interface as well as quantitative estimates of the temperature-dependent anisotropic interfacial diffusion coefficients D_{\parallel} and D_{\perp} . Molecular trajectories exhibited intermittent hopping, which was anisotropic at the interface with a nematic phase but isotropic when in contact with the isotropic phase. Interestingly, the interfacial diffusion anisotropy, $\frac{D_{\parallel}}{D_{\perp}}$, was virtually identical to that of self-diffusion in the bulk nematic phase, suggesting that the probe molecules sampled the structural properties of the adjacent bulk phase during their interfacial motion. Together, these observations were consistent with a model where molecules detached from the interface and executed three-dimensional “flights” into the bulk and reattached to the surface. Increased waiting times at lower temperatures significantly influenced the magnitude of the interfacial diffusion, explaining the dramatic decrease of the surface diffusion coefficients (compared to the relatively modest decrease of self-diffusion in the bulk) while the diffusion anisotropies remained consistent. Extension of this study to more exotic liquid crystal phases, such as smectics and lyotropic systems, is underway.

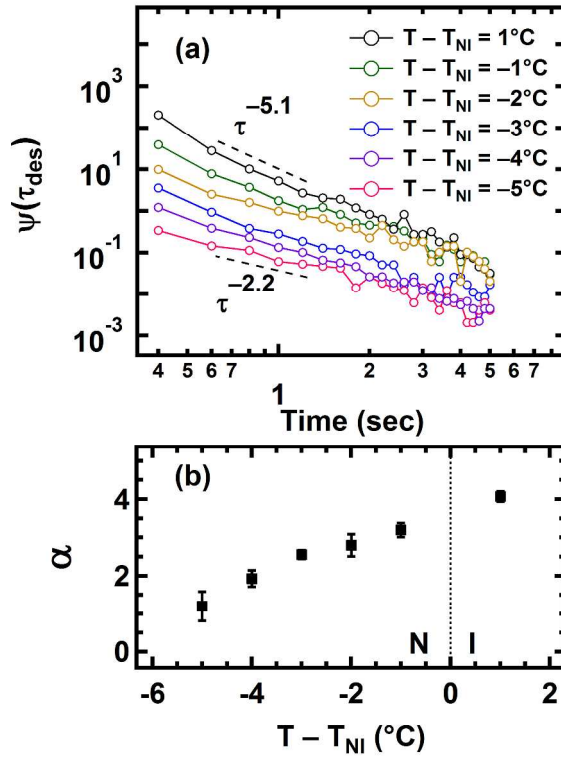


Figure 4. (a) Distributions of the waiting time between surface displacements. Markers with connecting lines are the experimental data at different temperatures (as annotated). Curves are vertically offset for clarity. Dashed lines beside the highest and lowest temperature data illustrate the approximate $\tau_{des}^{-(1+\alpha)}$ behavior of the respective distribution. (b) Temperature dependence of the fitting parameter α .

Our hope is that insights into the interfacial molecular transport of these exotic fluid systems will lead to an improved understanding of surface order and dynamics, ultimately leading to the development of new applications.

The authors gratefully acknowledge support from the National Science Foundation award #CBET-1160202 and from the Soft Materials Research Center (NSF-MRSEC DMR 1420736). Nathan Nelson acknowledges support from the U.S. Department of Energy Basic Energy Sciences, Chemical Science, Geosciences, and Biosciences Division (DE-SC0001854), who

provided support for the development and implementation of analytical models used to describe the experimental findings.

References

1. D. K. Schwartz, *Annu Rev Phys Chem*, 2001, **52**, 107-137; G. Ertl and H. J. Freund, *Phys Today*, 1999, **52**, 32-38; O. M. Braun and A. G. Naumovets, *Surf Sci Rep*, 2006, **60**, 79-158; A. M. Lieto, B. C. Lagerholm and N. L. Thompson, *Langmuir*, 2003, **19**, 1782-1787.
2. O. V. Bychuk and B. Oshaughnessy, *Phys Rev Lett*, 1995, **74**, 1795-1798.
3. O. Benichou, C. Loverdo, M. Moreau and R. Voituriez, *Rev Mod Phys*, 2011, **83**, 81-129.
4. A. Honciuc, A. W. Harant and D. K. Schwartz, *Langmuir*, 2008, **24**, 6562-6566.
5. R. Walder, N. Nelson and D. K. Schwartz, *Phys Rev Lett*, 2011, **107**; D. P. Wang, C. L. He, M. P. Stoykovich and D. K. Schwartz, *ACS Nano*, 2015, **9**, 1656-1664.
6. J. P. Bouchaud and A. Georges, *Phys Rep*, 1990, **195**, 127-293; J. Klafter and I. M. Sokolov, *First steps in random walks: from tools to applications*, Oxford University Press, 2011.
7. J. P. F. Lagerwall and G. Scalia, *Curr Appl Phys*, 2012, **12**, 1387-1412; R. R. Shah and N. L. Abbott, *J Am Chem Soc*, 1999, **121**, 11300-11310; J. Ma, X. Ye and B. Jin, *Displays*, 2011, **32**, 49-57.
8. P. Sheng, *Phys Rev A*, 1982, **26**, 1610-1617; P. Pieranski and B. Jerome, *Phys Rev A*, 1989, **40**, 317-322; Y. Ouchi, M. B. Feller, T. Moses and Y. R. Shen, *Phys Rev Lett*, 1992, **68**, 3040-3043.
9. Y. Bouligand, *Cr Chim*, 2008, **11**, 281-296.
10. H. Takezoe, M. Hara, S. Ichikawa and A. Fukuda, *Mol Cryst Liq Cryst*, 1985, **122**, 169-174.
11. S. V. Dvinskikh, I. Furo, H. Zimmermann and A. Maliniak, *Phys Rev E*, 2002, **65**, 61701-61701-61709.
12. D. Täuber and C. von Borczyskowski, *Int J Mol Sci*, 2013, **14**, 19506-19525.
13. T. Kawai, S. Yoshihara, Y. Iwata, T. Fukaminato and M. Irie, *Chemphyschem*, 2004, **5**, 1606-1609; T. Kawai, A. Kubota, K. Kawamura, H. Tsumatori and T. Nakashima, *Thin Solid Films*, 2008, **516**, 2666-2669.
14. Y. Gambin, G. Massiera, L. Ramos, C. Ligoure and W. Urbach, *Phys Rev Lett*, 2005, **94**, 110602; J. Bechhoefer, J. C. Geminard, L. Bocquet and P. Oswald, *Phys Rev Lett*, 1997, **79**, 4922-4925.
15. B. Schulz, D. Tauber, F. Friedriszik, H. Graaf, J. Schuster and C. von Borczyskowski, *Phys Chem Chem Phys*, 2010, **12**, 11555-11564; B. Schulz, D. Tauber, J. Schuster, T. Baumgartel and C. von Borczyskowski, *Soft Matter*, 2011, **7**, 7431-7440; M. Pampa and F. Cichos, *J Phys Chem B*, 2012, **116**, 14487-14493; D. Tauber, I. Trenkmann and C. von Borczyskowski, *Langmuir*, 2013, **29**, 3583-3593.
16. O. P. Pishnyak, S. Tang, J. R. Kelly, S. V. Shiyankovskii and O. D. Lavrentovich, *Phys Rev Lett*, 2007, **99**.
17. .
18. M. J. Skaug, J. Mabry and D. K. Schwartz, *Phys Rev Lett*, 2013, **110**.
19. L. Silvestri, L. Fronzoni, P. Grigolini and P. Allegrini, *Phys Rev Lett*, 2009, **102**; M. Niemann, H. Kantz and E. Barkai, *Phys Rev Lett*, 2013, **110**; S. Sadegh, E. Barkai and D. Krapf, *New J Phys*, 2014, **16**.
20. A. Clauset, C. R. Shalizi and M. E. J. Newman, *Siam Rev*, 2009, **51**, 661-703.

